*electronics*

MDPI

*Review*

# Novel Bio-Optoelectronics Enabled by Flexible Micro Light-Emitting Diodes

**Han Eol Lee**

Division of Advanced Materials Engineering, Jeonbuk National University, 567 Baekje-daero, Deokjin-gu, Jeonju 54896, Korea; haneol@jbnu.ac.kr; Tel.: +82-632702379

**Abstract:** Optical health monitoring and treatment have been spotlighted due to their biocompatible properties. Several researchers are investigating optical devices for obtaining health signals and curing diseases without any damage to the body. In particular, μLEDs have received a lot of attention as a future light source due to their superior optical/electrical properties, environmental stability, and structural advantages. According to their strengths, μLEDs have been used for various biomedical applications, such as optogenetics and hair regrowth. In this paper, we introduce the research tendency of μLEDs and the latest bio-applications.

**Keywords:** micro light-emitting diodes; biomedical devices; light-induced therapy; flexible and wearable electronics

check for updates

**Citation:** Lee, H.E. Novel Bio-Optoelectronics Enabled by Flexible Micro Light-Emitting Diodes. *Electronics* **2021**, *10*, 2644. https://doi.org/10.3390/electronics10212644

Academic Editor: Giovanni Andrea Casula

Received: 24 September 2021
Accepted: 27 October 2021
Published: 29 October 2021

**Publisher's Note:** MDPI stays neutral with regard to jurisdictional claims in published maps and institutional affiliations.

**Copyright:** © 2021 by the author. Licensee MDPI, Basel, Switzerland. This article is an open access article distributed under the terms and conditions of the Creative Commons Attribution (CC BY) license (https://creativecommons.org/licenses/by/4.0/).

## 1. Introduction

With the beginning of the Internet of Things (IoT) era, novel methods for efficient information utilization to handle and share various kinds of information in daily life have been discussed [1–14]. According to these requirements, academia and industries are attempting to narrow the physical/psychological distance between users and information, which is expected to be enabled by developing and commercializing various smart devices, including smart watches, home appliances, cell phones, and glasses. In other words, there has been a considerable amount of effort to realize a human–machine interface (HMI) in various aspects [15–19].

Since modern people are accustomed to lots of information, the desire to check their body/disease information in order to easily monitor and treat them has increased. These needs have been directly applied to newly develop smart devices. For example, smart devices can monitor various biometric information, such as pulse, heartbeat, and oxygen saturation, and then analyze living patterns (e.g., exercise and sleep and) in real time, helping to manage personal health [20–25]. For sustainable health monitoring and treatment, users have to continuously carry or wear the smart device obtaining information. However, these devices still have a critical limitation: huge equipment size, which is due to the intrinsic large volume of components, including batteries, circuits, and displays. In this regard, healthcare devices with a new form factor have been spotlighted, creating competition for the leading position in this fierce industry.

Recently, light-induced monitoring and treatment have attracted a lot of attention because of their biocompatibility, high therapeutic efficiency, and less-invasive process [26–30]. Since light-based healthcare devices collect accurate, vital information or efficiently cure physical illnesses without tissue damage, numerous medical teams are actively utilizing lasers or bulk light-emitting diodes (LEDs) as therapeutic equipment. However, this equipment has some drawbacks, such as its huge size, low power efficiency, high cost, and difficulty of frequent uses, as shown in Figure 1.

| | LASER | Bulk LED | MicroLED |
|---|---|---|---|
| **Output power** | Proportional to current above threshold | Linearly proportional to current | Linearly proportional to current |
| **Response time** | Fast | Slow | Medium |
| **Lifetime** | Long | Long | Long |
| **Device Size** | Extremely huge | Large | Small |
| **Power efficiency** | Low | Medium | High |
| **Cost** | Extremely expensive | Cheap | Medium |
| **Ease of Use** | Hard | Easy | Easy |

**Figure 1.** Comparison of LASER, bulk LED, and μLED as a light source for biomedical applications (red: disadvantages, blue: advantages).

Therefore, several researchers around the world have tried to miniaturize these phototherapy devices to ensure user-friendliness, convenience, and sustainable use. Among various light sources such as organic LEDs (OLEDs), quantum dot (QD)-based LEDs (QLEDs), and bulk LEDs, compound semiconductor-based inorganic microLEDs (μLEDs) have been considered as a next generation novel light source for biomedical applications because of their high brightness, superior power efficiency, fast response time, and excellent stability [7,10,17,31–35]. In particular, μLEDs can be easily manufactured into free form factor optoelectronic devices due to their ultra-small size, showing the advantage of flexibility and the possibility for wearable biomedical applications. According to these advantages, the μLEDs have been applied to various bio-applications such as optogenetics, vital monitoring, and hair loss treatment. In this paper, we introduce the state-of-the-art research results of μLEDs and their investigation trends for biomedical applications.

## 2. Flexible Micro Light-Emitting Diodes

The μLED has been spotlighted as a novel fusion technology of information technology (IT) and nanotechnology (NT) and is proposed as the next-generation light source to solve numerous problems of existing OLED and QLED displays (e.g., afterimage, burn-in effect, heat/water instability, and slow response time). Figure 2 shows a comparison table among QLED, OLED, and μLED displays in terms of their emission type, thickness, optical property, lifetime, and cost. The μLEDs are self-emissive light sources with high brightness and a longer lifetime than OLED and QLED, and display excellent image quality. In particular, μLEDs of extremely small size (width from 10 to 100 μm and thickness under 5 μm) have superior optical/electrical properties, such as excellent luminescence efficiency over 100 lm $W^{-1}$, strong illumination over $10^5$ cd $m^{-2}$, high color contrast, and superior power efficiency.

| | QLED | OLED | MicroLED |
|---|---|---|---|
| Type | Backlight/LED | Self-emissive | Self-emissive |
| Thickness | Thick | Thin | Thin |
| Brightness | Medium | Low | High |
| Contrast ratio | Low | High | High |
| Lifetime | Medium | Short | Long |
| Image quality | Low | High | High |
| Cost | Low | High | High |

**Figure 2.** Comparison of QLED, OLED, and μLED display in terms of structure, optical/electrical properties, lifetime, and cost (red: disadvantages, blue: advantages).

Therefore, in the display industry, it is predicted that high-performance μLEDs will even enter fine-pitch display fields that are dominated by OLEDs and QLEDs, as shown in Figure 3. Despite several advantages of μLEDs, there are still some challenges in realizing commercialization, such as efficient packaging, chip structure innovation, and development of a new transfer methodology.

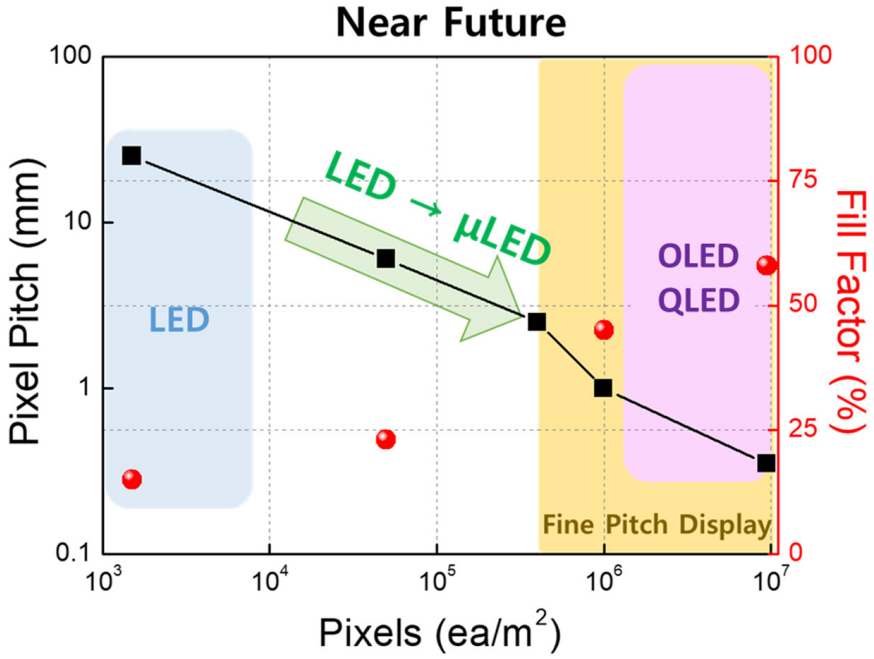



**Figure 3.** Development prospect of light sources as display components.

First, flexible μLEDs are fabricated as follows [11,35–39]: III-V compound semiconductor layers are grown by metalorganic chemical vapor deposition (MOCVD), metalorganic vapor-phase epitaxy (MOVPE), or molecular beam epitaxy (MBE) on the mother substrate (e.g., silicon, GaAs, and sapphire), forming a thin-film LED structure with a p-type material, a multi quantum well (MQW), and an n-type material. The epitaxial layers are etched into numerous microscale chips through micro-electromechanical systems (MEMS) processes.

The LEDs on the mother substrate are selectively peeled off and placed into a specific position on a target substrate. Finally, the μLEDs are electrically connected and packaged for passivating the device from environmental stresses.

The μLEDs can typically be divided into three types (Figure 4). There are fully packaged bulk LEDs, as well as lateral- and vertical-structured μLEDs, which are made by III-V or III-N compound semiconductors on epitaxial substrate (e.g., III-V: GaAs; III-N: Si, SiC, and sapphire). They have different characteristics in thermal, electrical, and optical properties, resulting from structural differences of bulk/thin-film and electrode location. Lateral μLEDs have a long current path of about 50~100 μm between electrodes, whereas vertical μLEDs have a short current path under 5 μm, inducing negligible Joule heating during device operation. Thanks to this structural advantage, vertical-structured microLEDs have various superiorities compared to others, including a small size, a fast/cheap process, superior electrical/thermal properties, and simple wiring. Particularly, vertical-structured μLEDs with low heating are most suitable to realize biomedical applications due to their thermally noninvasive property.

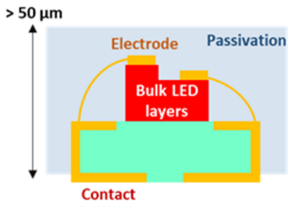
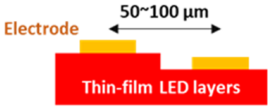
| | Bulk LED | Lateral MicroLED | Vertical MicroLED |
|---|---|---|---|
| **Material** | III-V or III-N compound semiconductor | | |
| **Structure** |  |  |  |
| **LED type** | Fully-packaged chip | Thin film | Thin film |
| **Size** | Height > 50 μm | Height < 5 μm | Height < 5 μm |
| **Process** | Slow & Expensive | Fast & Cheap | Fast & Cheap |
| **Power consumption** | Low | High | Low |
| **Heating** | Low | High | Low |
| **Wiring** | Complex | Complex | Simple |

**Figure 4.** Comparison of bulk LED, lateral-, and vertical-structured μLEDs; red: disadvantages, blue: advantages).

As mentioned above, the processes, i.e., the transfer technology of numerous μLED chips from the mother wafer to the target substrate, are the most important factors for developing μLED-based electronic systems, such as displays, biomedical therapeutic devices, and healthcare sensors. Since the transfer efficiency is directly related to the device yield, manufacturing time, and unit cost, several researchers around the world have attempted to transfer thin-film μLED chips through various methods. The polydimethylsiloxane (PDMS)-based pick-and-place method was the most widely used for μLED transfer. The μLED chips were attached to sticky PDMS by van der Waals adhesive force and released onto the adhesive-coated target substrate. Furthermore, although various approaches, such as electrostatic or electromagnetic force-based transfer, were suggested as new transfer methods, they still had many problems, including thermal/electrical damage to the LED layers, slow transfer speed, and difficulty in large-area processing. Recently, novel tech-

nology was proposed by using an anisotropic conductive film (ACF) [32,35,40]. Thin-film μLEDs were simultaneously attached and packaged with the target substrate through ACF by applying heat and pressure. The ACF-based transfer was performed with a rapid process speed, high yield, and large-area transfer, enabling electrical connection with complicated electrodes at the same time as the μLED transfer.

Figure 5a shows a self-powered flexible μLED array on a flexible plastic film. Jeong et al. made a flexible μLED array by transferring from a gallium arsenide (GaAs) wafer to a polyimide (PI) substrate by using the ACF transfer/packaging method [32]. Finally, μLEDs were integrated with a flexible piezoelectric energy harvester to complete a self-powered display system. Figure 5b indicates a flexible 3 × 3 μLED array in a bent state (bending curvature radius of 5 mm) illuminating brilliant light. Figure 5c is a luminance–current–voltage (L–I–V) graph of the fabricated flexible μLED. As shown in the bottom inset image, the 3 × 3 μLED arrays were driven by a ~3 V, emitting red light with a wavelength of 653 nm. When mechanical force was applied to the thin-film piezoelectric material (lead zirconate titanate) of the device, the energy harvester generated an electrical power for operating a flexible μLED array without any external power source. The μLEDs were repeatedly turned on and off by the pulsed electrical power from the energy generator, as depicted in the upper inset graph of Figure 5c.

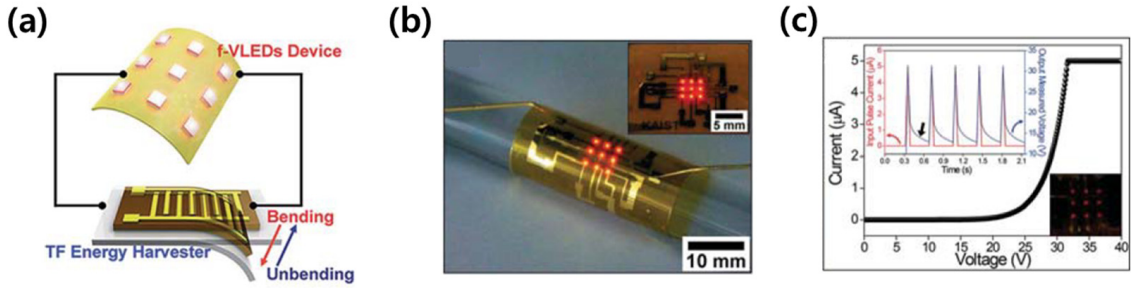



**Figure 5.** (**a**) Schematic image of self-powered flexible μLEDs that were composed of flexible red μLEDs and a thin-film piezoelectric power generator. (**b**) Photograph of flexible red μLED array. The inset image is a top view of the device. (**c**) I-V curve of flexible μLED arrays. The top inset shows output current and voltage from a thin-film energy harvester. The bottom inset indicates flexible red μLEDs, operated by a piezoelectric energy harvester. Reproduced with permission [32]. Copyright 2014, Royal Society of Chemistry.

Figure 6a displays a monolithic flexible GaN μLED array with a 30 × 30 passive-matrix circuit [31]. Lee et al. developed the monolithic fabrication process for flexible, vertical-structured μLEDs (f-VLEDs). The GaN μLED array was fabricated on a rigid sapphire wafer and then exfoliated with a laser lift-off process. The freestanding GaN μLED array was isolated with epoxy-based polymer. After the electrical interconnection of μLED chips by a silver nanowire (AgNW)-based electrode, the device was passivated by the biocompatible parylene-C layer. After flipping over the device, the AgNW top electrode was made on the device. As shown in the inset images of Figure 6a, the high-density blue μLED array with passive-matrix structure was operated at a bending curvature radius of 5 mm. Since the device was electrically connected by a transparent AgNW network, the μLEDs in off-state were invisible on the human fingernail (Figure 6b and its inset image). According to heat flux simulation, flexible vertical μLEDs had superior thermal stability compared to flexible lateral μLEDs due to efficient heat dissipation through the bottom electrode. The GaN f-VLED displayed excellent mechanical durability during $10^5$ bending/unbending cycles because its mechanical neutral plane was placed at the center of μLED chips (Figure 6c). Furthermore, the device lifetime was expected to last 11.9 years. In accordance with these results, monolithic f-VLEDs are anticipated to commercialize in the display and biomedical device fields.

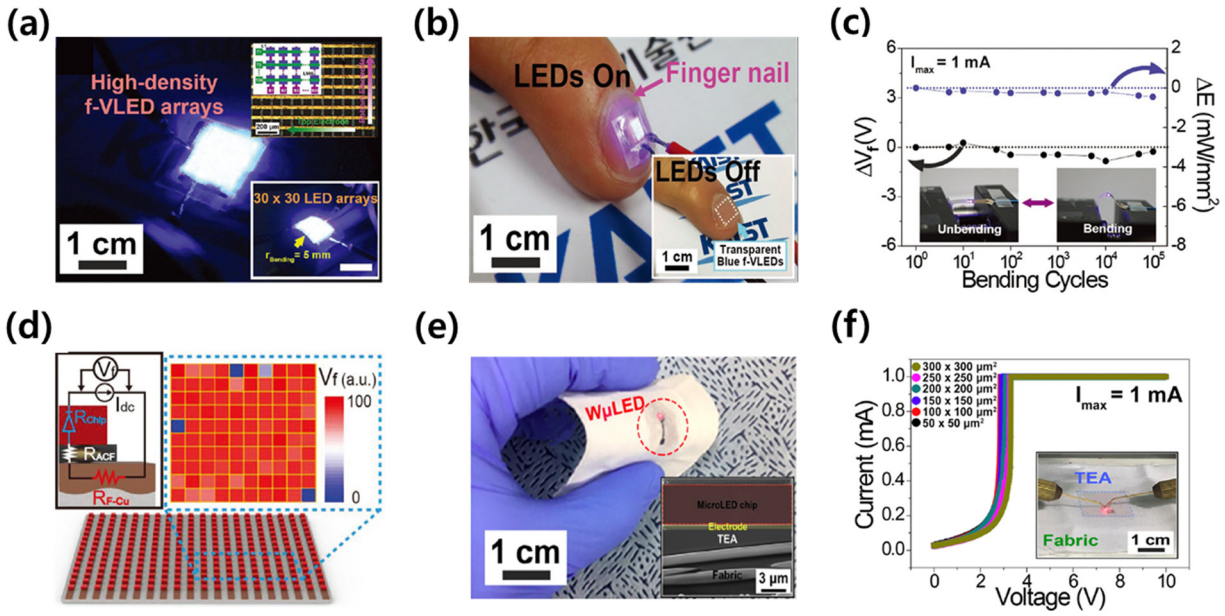



**Figure 6.** (**a**) Photograph of monolithic flexible blue μLEDs with 30 × 30 array. The top inset is a magnified optical image of a passive-matrix μLED array. Scale bar: 1 cm. The bottom inset is an optical image of monolithic blue μLEDs in a bent state. (**b**) Transparent flexible blue μLEDs on human fingernail. The inset image shows fingernail-attached transparent device in off-state. (**c**) Fatigue test results of monolithic flexible μLEDs during $10^6$ bending/unbending cycles. Reproduced with permission [31]. Copyright 2018, Wiley-VCH. (**d**) Normalized forward voltage of 50 × 50 μLED arrays with flash-induced Cu electrodes. Reproduced with permission [35]. Copyright 2021, Wiley-VCH. (**e**) Optical image of wearable red μLED on fabric substrate. The inset is a cross-sectional SEM image of wearable μLED. (**f**) I-V characteristics of wearable μLEDs with various size. Reproduced with permission [34]. Copyright 2019, Elsevier.

Shin et al. investigated robust Cu electrodes for μLED display applications [35]. Although Cu-based electrodes were spotlighted for application in display circuits due their cheap price, robustness, and high conductivity, Cu had a critical delamination issue on rigid glass substrate. Shin et al. resolved this issue through flashlight-induced Cu-glass interlocking. By radiating a high-powered flashlight on CuO nanoparticles, the CuO was reduced to a conductive Cu layer, simultaneously forming strong adhesion with glass. The 50 × 50 μLED arrays were interconnected with a flash-inducted robust Cu electrode by a thermo-compressive ACF bonding process. The developed device showed thermal/humid stability and high uniformity in large-scale μLED arrays, as shown in Figure 6d. Lee et al. developed wearable μLEDs (WμLEDs) on a 100% cotton fabric [34]. WμLEDs were fabricated using the same protocol with monolithic f-VLED and transferred through transparent elastomeric adhesive by the thermo-compressive process. Figure 6e displays WμLEDs emitting red light at a bent state. The attachment stability between μLED chips and fabric was sophisticatedly investigated by finite element method (FEM) simulation, tensile tests, peel-off tests, digital image correlation (DIC) analysis, and bending fatigue tests. As shown in Figure 6f, WμLEDs with various chip sizes were operated at a forward voltage of ~2.8 V. The WμLEDs showed potential for outdoor application through chemical, thermal, humid, and artificial sunlight tests.

## 3. Optogenetic Stimulators

Various electrical/magnetic stimulations have been widely used to treat physical or mental diseases of living animals [41–47]. For example, Hwang et al. developed an artificial pacemaker using a piezoelectric material-based electrical energy harvester. The developed device controlled the heartbeat of a living mouse by directly stimulating the heart [48]. In addition, an electrical stimulator, which was made by flexible piezoelectric thin-film, was inserted into the motor cortex of a living mouse. The device generated electrical stimulation for commanding artificial movement of mouse forelimbs [49]. However, in the

case of these invasive electrical/magnetic stimulation methods, there were some critical drawbacks, such as a large surgery needed for device implantation and thermal damage of living tissue.

To resolve the problems of electrical/magnetic therapeutic methods, numerous researchers have investigated light-based neural stimulation, which is well known as optogenetics [50–53]. Figure 7a displays an experimental setup of single cell-scaled optogenetic control on a high-density 4 × 4 μLED array [41]. Mao et al. optogenetically manipulated $Ca^{2+}$ signal from sub-10 μm human embryonic kidney 293 (HEK 293) cells by using high-performance μLEDs. After co-expressing ChR2 (optogenetic actuator) and jRCaMP1a ($Ca^{2+}$ indicator) to HEK 293 cells, the cells were closely located on a μLED array to confirm the spatial resolution of μLED-based optogenetic stimulation (Figure 7b). Despite the short distance (sub-5 μm) between two cells, cell 3 was only stimulated by red μLED pixels 5 and 9, not pixel 14, as shown in the $\Delta F/F_0$ graph of Figure 7c. The results indicated that μLED-based optogenetic control with high spatial resolution can be utilized not only in pharmaceutical screening studies by lab-on-a-chip but also in single-cell investigations in deep tissues.

μLEDs have been applied to optical stimulations for cultured cells as well as living animals. Kim et al. developed a needle-shaped μLED device to investigate peripheral neural pathways by using optogenetic signal analyses [42]. The μLED was fabricated on a copper-polyimide (Cu-PI) substrate with a needle structure, which was integrated with a wireless radio frequency (RF) power system (Figure 7d). After device passivation with a biocompatible polymer, the wireless optogenetic device was implanted inside a mouse stomach to investigate the gastrointestinal nerves, as shown in Figure 7e. The fully integrated wireless optogenetic device successfully stimulated the genetically manipulated vagal neurons in the mouse stomach, showing peripheral nerve connectivity and functionality of mucosal sensors for suppressing food ingestion. The PI-embedded μLED device was stably operated during in vivo experiments with various stimulating parameters. The developed multimodal μLED device was easily implanted and simply set up in <60 min, reducing its production cost and experimental time. In addition, this novel system can be widely applied to operate optogenetic stimulation experiments for the periphery, brain, or other organs. Figure 7f shows a representative example of applying optogenetics to a cochlear implant [43]. Dieter et al. implanted a needle-type optogenetic stimulator into the mouse brain for optically stimulating spiral ganglion neurons and compared the results with electrical and acoustic stimulations. Brain stimulation by a needle-type μLED device showed the most similar optogenetic results with acoustic stimulation and confirmed the possibility of selective optical activation of the auditory organ. The developed optical device used a limited excitation of spiral ganglion neurons compared to electrical stimulation. Figure 7g indicates a wireless, implantable, and optogenetic pacemaker implanted on a rat heart [44]. This multimodal device provided the usability of wireless, battery-free functions for chronically implantable applications. The fabricated optogenetic pacemaker showed successful animal pacing during free movements, without any device degradations. Furthermore, the device solved critical drawbacks of the existing optogenetic pacemakers, such as spatiotemporal accuracy and use of multimodal optoelectrodes. In particular, genetically modified animals were optogenetically controlled and paced by a device, simultaneously, in various frequencies. As described above, needle-shaped μLED optogenetic devices have been studied in various forms for several years and applied to actual living animals.

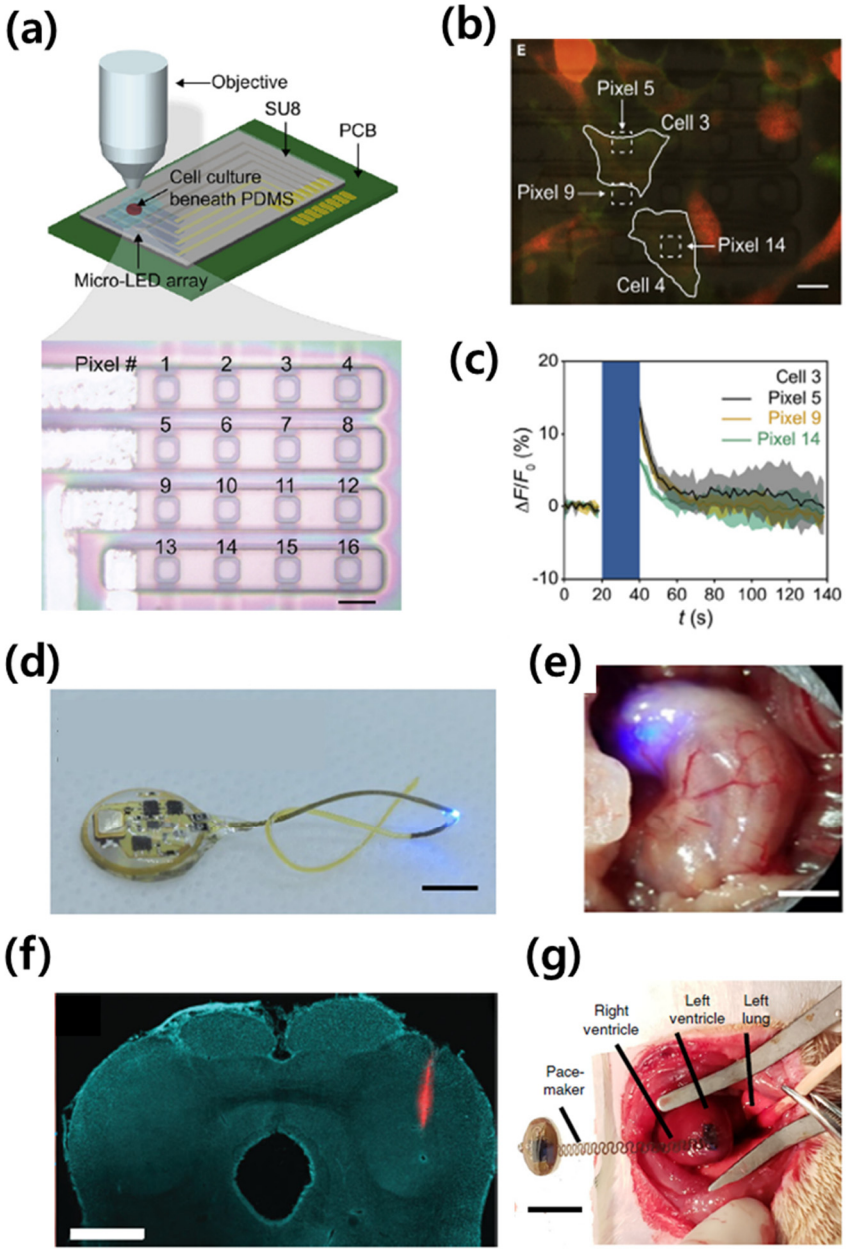



**Figure 7.** (**a**) Schematic image of experimental setup for μLED-based cell imaging. (**b**) A magnified optical microscopic image of ChR2 (green, optogenetic actuator)-jRCaMP1a (red, $Ca^{2+}$ indicator)-expressed cells on 4 × 4 μLED array. Scale bar: 10 μm. (**c**) Fluorescence intensity ratio ($\Delta F/F_0$) graph of cell 3 on μLED pixels (pixel 5, 9, and 14) after optogenetic stimulations. Reproduced with permission [41]. Copyright 2019, Elsevier. (**d**) Optical image of wireless gastric optogenetic implant device. Scale bar: 5 mm. (**e**) Photograph of the implanted wireless optogenetic device with blue light in the mouse stomach. Reproduced with permission [42]. Copyright 2021, Springer Nature. (**f**) Coronal section image of mouse brain, showing DAPI-stained brain tissue region (cyan) and Dil-stained electrode region (red). Reproduced with permission [43]. Copyright 2019, Springer Nature. (**g**) Image of wireless multimodal optogenetic stimulator, which was sutured on left ventricle of the rat. Reproduced with permission [44]. Copyright 2019, Springer Nature.

Tajima et al. suggest a ring-structured wireless optogenetic stimulator for protecting animal obesity [54]. Figure 8a displays a freely moving mouse implanted with a μLED-based wireless optogenetic device. As shown in Figure 8b, the miniaturized device (2 $mm^3$ size) was composed of an electrical power transferring coil, a power rectifying circuit, and a μLED, which were passivated by a biocompatible parylene-C. After implanting the device

into subcutaneous adipose tissue on the mouse, it freely moved on honeycomb-structured transmitters, operating a blue μLED by ~3 mW transferred power. Figure 8c indicates the tissue weight of Adipo-ChR2 mice (genetically modified mice for optogenetic control) and controls, and hematoxylin and eosin (H&E)-stained tissue images. After periodic optical stimulations (10 min pulse with 10 Hz) for 23 consecutive days, Adipo-ChR2 mice showed decreased fat mass compared to control mice. In this work, although the optogenetic device successfully modulated adipocytes in a living mouse, there were still some limitations, such as tissue damage due to the invasive device and the large surgery for device implantation.

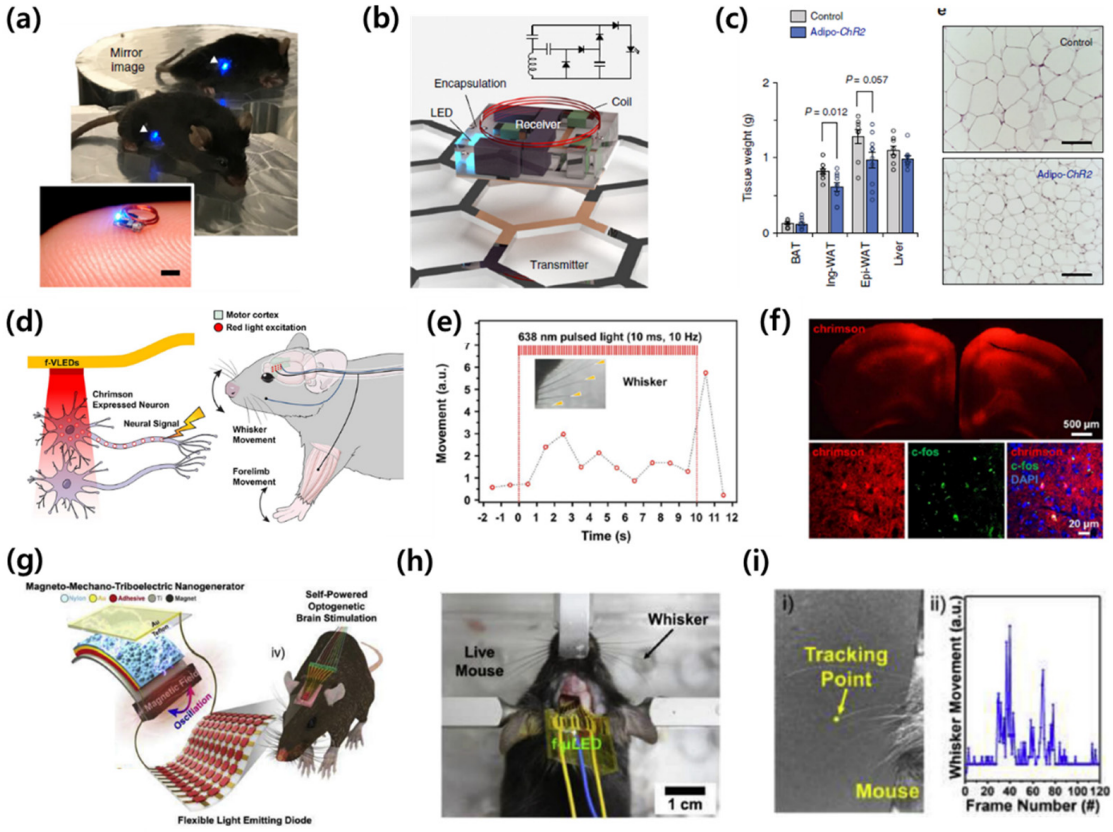



**Figure 8.** (**a**) Photograph of a freely moving mouse with an implanted wireless optogenetic device. The inset shows a wireless implantable optogenetic device on a human fingertip. Scale bar: 1 mm. (**b**) Illustration of the wireless implantable optogenetic device with circuit diagram, which was composed of μLED and power receiver coil. (**c**) Tissue weight comparison of Adipo-ChR2 mice and littermate controls. Right images show hematoxylin and eosin (H&E) staining of the inguinal white adipose tissue (WAT) after light stimulations (Control, n = 8; Adipo-ChR2, n = 10). Reproduced with permission [54]. Copyright 2020, Springer Nature. (**d**) Schematic illustration of optogenetic brain stimulation for modulating mouse behaviors, which was fulfilled by flexible red μLEDs. (**e**) Tracking graph of mouse whisker movement for 10 ms stimulation by red light. (**f**) Confocal images of the sliced mouse brain after optogenetic stimulation. Top image shows chrimson-expressed frontal motor cortex. Bottom images indicate cortical neurons, which were co-expressed by chrimson (red) and c-fos (green). Reproduced with permission [40]. Copyright 2018, Elsevier. (**g**) Schematic illustration of self-powered optogenetic stimulation by flexible μLEDs and a magneto-mechano-triboelectric nanogenerator. (**h**) Experimental image for optogenetic brain stimulation, showing implantation of flexible μLEDs under the anesthetized mouse skull. (**i**) Tracking of mouse whisker movement during self-powered optogenetic stimulation. Reproduced with permission [17]. Copyright 2020, Elsevier.

In order to overcome the disadvantages of the aforementioned invasive optogenetic device, a flexible μLED-based optogenetic stimulator has been developed as a novel neurostimulation method. In this simple method, a flexible μLED array was smoothly inserted through a small slit in an animal skull and conformally attached onto a brain surface for two-dimensional stimulation of its cerebral cortex. Figure 8d displays an

experimental scheme of flexible μLED-based optogenetic stimulation [40]. The device was implanted using a noninvasive method, and irradiated red light was used to activate ChR2-expressed neurons in the mouse's motor cortex. By using a vertical-structured flexible μLED with a short current path for in vivo experiments, although a strong light of 30 mW $mm^{-2}$ was directly emitted onto the brain surface, there was no thermal or mechanical tissue damage. Figure 8e indicates the movement tracking of a living mouse whisker after artificial optical stimulation. There were little whisker movements without light irradiation, while there were mm-scaled dynamic movements after red light stimulation (wavelength of 650 nm). After in vivo experiments, the mouse brain was slightly sliced for tissue analysis. As shown in Figure 8f, chrimson (ChR2) was successfully expressed in the frontal motor cortex of the mouse. Lee et al. optogenetically stimulated the motor cortex of the mouse brain by using flexible μLEDs and a magneto-mechano-triboelectric nanogenerator (MMTEG), as shown in Figure 8g [17]. By scavenging a stray magnetic field from home appliances, MMTEG generated a voltage of 237 V and current of 33 μA, operating a flexible red μLED array. The flexible μLED had an enhanced power efficiency by minimizing the contact resistance between metal electrodes and LED chips through an ohmic contact. Figure 8h indicates an experimental image of an anesthetized and fixed mouse with an implanted optogenetic stimulator. The red light from the μLEDs stimulated and activated cortical motor neurons in the mouse's motor cortex with 10 ms pulses at 60 Hz frequency, successfully creating artificial movements of the whiskers (Figure 8i).

## 4. Other Biomedical Applications

Flexible μLEDs have been used in various forms of wearable medical patches due to their excellent biocompatibility, low heating, and excellent mechanical/chemical/thermal stability. According to these advantages, flexible μLED-based patches have been widely applied to treat chronic skin diseases or monitor human vital signs. For example, blood oxygen saturation (SpO2), heartbeat, and glucose levels in blood were continuously tracked [44,55,56]. Lee et al. developed a high-performance red flexible μLED (30 × 30 array) and utilized it as a wearable patch for hair regrowth application [33]. The red μLED exhibited a superior light irradiance of 30 mW $mm^{-2}$ with low heating. Since the device was not heated over 40 °C, the developed flexible μLED-based patches were directly attached onto the skin for a few days. The patch had an ultrathin thickness of 20 μm and stably operated during harsh $10^5$ bending fatigue tests. Figure 9a shows a schematic 3D illustration of a flexible μLED-based patch for mouse hair regrowth. Hair growth experiments were conducted for 20 consecutive days in three groups: a negative control group (no treatment), a chemically treated group (minoxidil), and a μLED experiment group. The experiment was carried out using mice without dorsal hairs under the same conditions.

As shown in Figure 9b, the LED light-treated group showed the best curative effect among the three groups, showing a fast and large hair regrowth area for 20 days. Figure 9c indicates magnified optical images of mouse dorsal hairs in three groups after biomedical experiments. The light-treated hair was the thickest and longest compared to other groups. For verification of hair follicles in the skin tissue after bio-experiments, the mouse skin was extracted to perform histological and immunofluorescence analyses (Figure 9d). In hematoxylin and eosin (H&E) images, the LED light-irradiated skin tissue had more hair follicles (purple color) than those in the control groups. β-catenin, which is closely related to hair follicle proliferation, was dominantly expressed in the flexible μLED group. This result came from efficient stimulation of hair follicles by red light (630 nm wavelength), because the red light penetrated 1~2 mm below the mouse skin, effectively stimulating the hair follicles to grow hair.

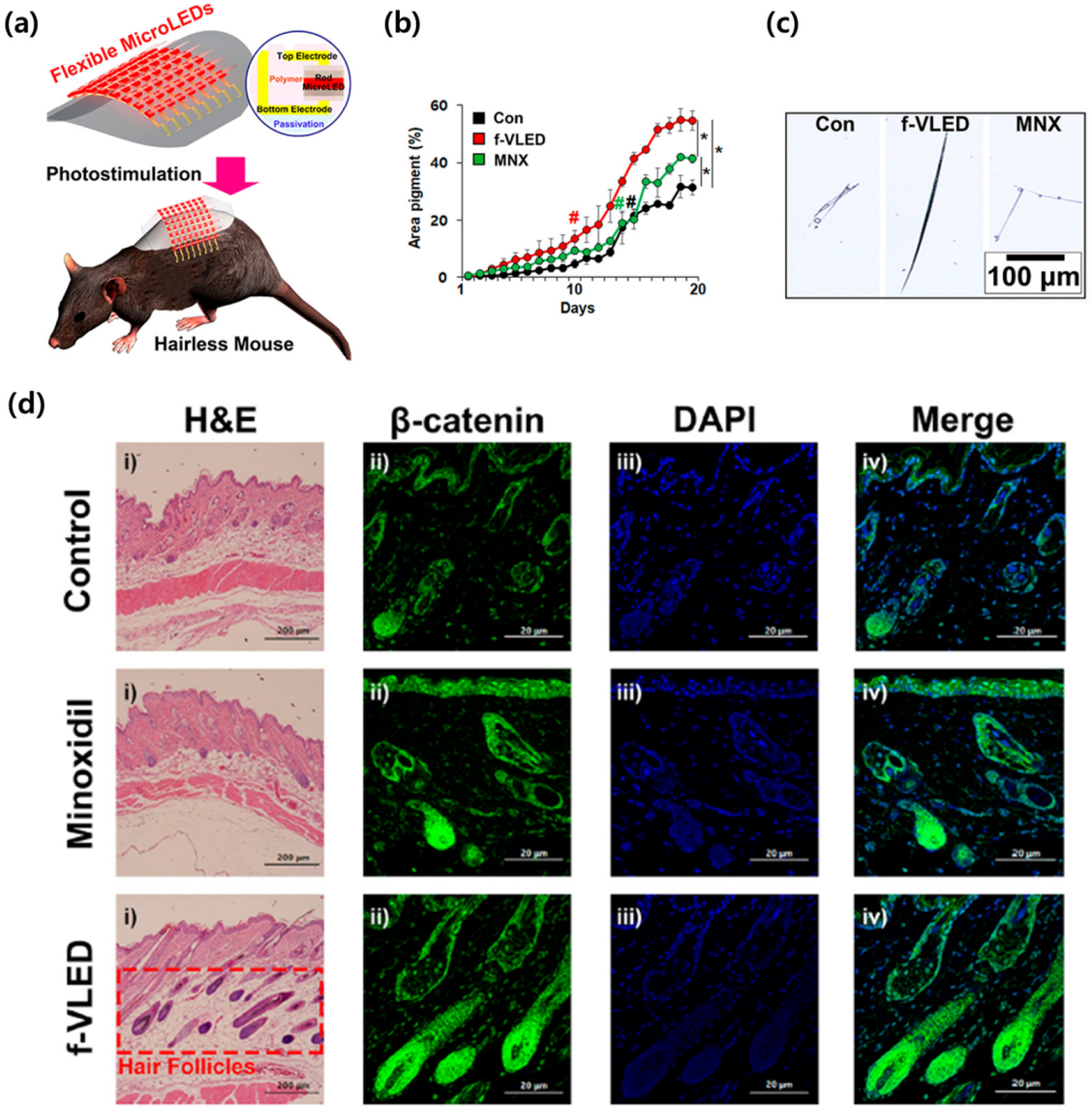



**Figure 9.** (**a**) Schematic illustration of trichogenic photostimulation by flexible red μLED patch. (**b**) Areal trend of hair regrowth for 20 consecutive days. ($p < 0.05$, paired $t$ test, # $p < 0.05$, two way ANOVA; * $p < 0.01$, *** $p < 0.001$, paired $t$ test)(**c**) Magnified microscopic images of mouse dorsal hair after trichogenic stimulation tests. (**d**) Histological and fluorescence images of mouse skin after 20 days of trichogenic stimulation tests. Reproduced with permission [33]. Copyright 2018, American Chemical Society.

## 5. Conclusions

With the advent of the hyperconnected IoT era, modern people have been interested in their healthcare and treatment of acute and chronic diseases. Until now, however, there has only been a therapeutic method in which a patient could directly visit a hospital and receive treatment from medical staff. Furthermore, they need to utilize huge and heavy therapeutic equipment in a designated place. In order to solve these problems, novel types of therapeutic devices have been developed in wearable/flexible forms. In addition, the developed devices have been implanted in various body parts, resulting in numerous biological, meaningful results.

In particular, light-based wearable biomedical devices, which are considered as creative convergence electronic devices in IT, BT, and NT, have the advantage of enabling continuous treatment without damage to the body. However, existing organic-based optoelectronic devices are exceptionally vulnerable to heat/moisture. Therefore, it is essential to develop a wearable biomedical device using μLED, which is well known as a

display light source and biocompatible device with excellent opto-electrical properties as well as environmental stability. In this paper, overall μLED technology is introduced to achieve next-generation biotherapeutic applications. As representative biomedical fields, neuromodulation and hair regrowth were explained, showing a superior treatment effect compared to the existing chemical/electrical/magnetic stimulation. As shown in Figure 10, μLED-based devices have been used not only for the introduced applications but also for low-power sensors and patches for skin beauty (e.g., whitening and anti-aging). Despite these research efforts, flexible/wearable μLEDs are at an early stage with many issues to be solved, such as integration with other devices and power supply. In addition, from the industrial perspective, expensive raw materials, process costs, and difficulties in large-scale production are also issues that must be addressed in the future. Nevertheless, μLED-based patches are currently being researched and developed with international research groups and global companies with outstanding results. By solving the above-mentioned problems and moving onto a bio-friendly patch form, it is expected that oxygen saturation (SpO2) sensors, glucose sensors for diabetic patients, and skin patch for treatment of chronic skin diseases (e.g., acne, psoriasis, and skin cancer) will be developed. If this kind of progress is made in the future, novel μLED technology will be established as a new industrial field in the smart healthcare field as well as in the display field.

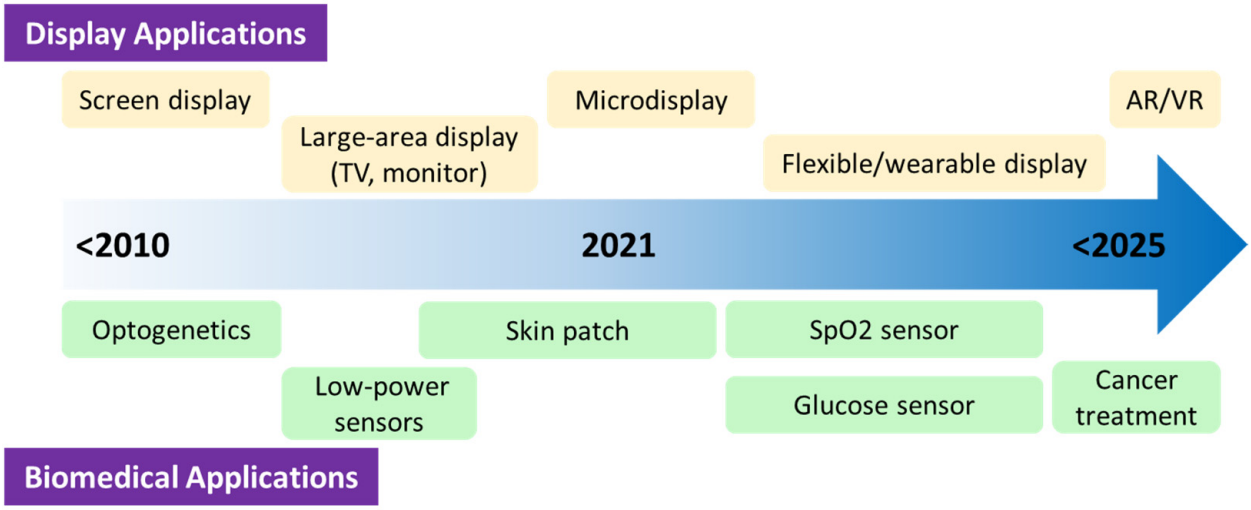



**Figure 10.** Development roadmap of μLEDs for display and biomedical applications.

**Funding:** This paper was supported by research funds for newly appointed professors of Jeonbuk National University in 2021.

**Conflicts of Interest:** The author declares no conflict of interest.

## References

1. Lee, H.E.; Park, J.H.; Kim, T.J.; Im, D.; Shin, J.H.; Kim, D.H.; Mohammad, B.; Kang, I.-S.; Lee, K.J. Novel Electronics for Flexible and Neuromorphic Computing. *Adv. Funct. Mater.* **2018**, *28*, 1801690. [CrossRef]
2. Joe, D.J.; Kim, S.; Park, J.H.; Park, D.Y.; Lee, H.E.; Im, T.H.; Choi, I.; Ruoff, R.S.; Lee, K.J. Laser-Material Interactions for Flexible Applications. *Adv. Mater.* **2017**, *29*, 1606586. [CrossRef]
3. Kim, S.J.; Lee, H.E.; Choi, H.; Kim, Y.; We, J.H.; Shin, J.S.; Lee, K.J.; Cho, B.J. High-Performance Flexible Thermoelectric Power Generator Using Laser Multiscanning Lift-Off Process. *ACS Nano* **2016**, *10*, 10851–10857. [CrossRef] [PubMed]
4. Lee, H.; Lee, H.E.; Wang, H.S.; Kang, S.; Lee, D.; Kim, Y.H.; Shin, J.H.; Lim, Y.; Lee, K.J.; Bae, B. Hierarchically Surface-Textured Ultrastable Hybrid Film for Large-Scale Triboelectric Nanogenerators. *Adv. Funct. Mater.* **2020**, *30*, 2005610. [CrossRef]
5. Im, T.H.; Lee, C.H.; Kim, J.C.; Kim, S.; Kim, M.; Park, C.M.; Lee, H.E.; Park, J.H.; Jang, M.S.; Lee, D.C.; et al. Metastable quantum dot for photoelectric devices via flash-induced one-step sequential self-formation. *Nano Energy* **2021**, *84*, 105889. [CrossRef]
6. Wang, H.S.; Im, T.H.; Kim, Y.B.; Sung, S.H.; Min, S.; Park, S.H.; Lee, H.E.; Jeong, C.K.; Park, J.H.; Lee, K.J. Flash-welded ultraflat silver nanowire network for flexible organic light-emitting diode and triboelectric tactile sensor. *APL Mater.* **2021**, *9*, 061112. [CrossRef]

7. Lee, H.E.; Shin, J.H.; Lee, S.H.; Lee, J.H.; Park, S.H.; Lee, K.J. Flexible micro light-emitting diodes for wearable applications. In Proceedings of the Light-Emitting Devices, Materials, and Applications, San Francisco, CA, USA, 1 March 2019; Strassburg, M., Kim, J.K., Krames, M.R., Eds.; SPIE: San Francisco, CA, USA, 2019; p. 14.
8. Kim, S.J.; Choi, H.; Kim, Y.; We, J.H.; Shin, J.S.; Lee, H.E.; Oh, M.-W.; Lee, K.J.; Cho, B.J. Post ionized defect engineering of the screen-printed Bi 2 Te 2.7 Se 0.3 thick film for high performance flexible thermoelectric generator. *Nano Energy* **2017**, *31*, 258–263. [CrossRef]
9. Kim, D.H.; Lee, H.E.; You, B.K.; Cho, S.B.; Mishra, R.; Kang, I.; Lee, K.J. Flexible Crossbar-Structured Phase Change Memory Array via Mo-Based Interfacial Physical Lift-Off. *Adv. Funct. Mater.* **2019**, *29*, 1806338. [CrossRef]
10. Lee, H.E.; Shin, J.H.; Park, J.H.; Hong, S.K.; Park, S.H.; Lee, S.H.; Lee, J.H.; Kang, I.; Lee, K.J. Micro Light-Emitting Diodes for Display and Flexible Biomedical Applications. *Adv. Funct. Mater.* **2019**, *29*, 1808075. [CrossRef]
11. Park, J.H.; Lee, H.E.; Jeong, C.K.; Kim, D.H.; Hong, S.K.; Park, K.-I.; Lee, K.J. Self-powered flexible electronics beyond thermal limits. *Nano Energy* **2019**, *56*, 531–546. [CrossRef]
12. Jung, D.H.; Park, J.H.; Lee, H.E.; Byun, J.; Im, T.H.; Lee, G.Y.; Seok, J.Y.; Yun, T.; Lee, K.J.; Kim, S.O. Flash-induced ultrafast recrystallization of perovskite for flexible light-emitting diodes. *Nano Energy* **2019**, *61*, 236–244. [CrossRef]
13. Peng, Y.; Que, M.; Lee, H.E.; Bao, R.; Wang, X.; Lu, J.; Yuan, Z.; Li, X.; Tao, J.; Sun, J.; et al. Achieving high-resolution pressure mapping via flexible GaN/ ZnO nanowire LEDs array by piezo-phototronic effect. *Nano Energy* **2019**, *58*, 633–640. [CrossRef]
14. Kim, I.H.; Im, T.H.; Lee, H.E.; Jang, J.; Wang, H.S.; Lee, G.Y.; Kim, I.; Lee, K.J.; Kim, S.O. Janus Graphene Liquid Crystalline Fiber with Tunable Properties Enabled by Ultrafast Flash Reduction. *Small* **2019**, *15*, 1901529. [CrossRef] [PubMed]
15. Park, A.H.; Lee, S.H.; Lee, C.; Kim, J.; Lee, H.E.; Paik, S.-B.; Lee, K.J.; Kim, D. Optogenetic Mapping of Functional Connectivity in Freely Moving Mice via Insertable Wrapping Electrode Array Beneath the Skull. *ACS Nano* **2016**, *10*, 2791–2802. [CrossRef] [PubMed]
16. Lee, H.E.; Kim, S.; Ko, J.; Yeom, H.-I.; Byun, C.-W.; Lee, S.H.; Joe, D.J.; Im, T.-H.; Park, S.-H.K.; Lee, K.J. Skin-Like Oxide Thin-Film Transistors for Transparent Displays. *Adv. Funct. Mater.* **2016**, *26*, 6170–6178. [CrossRef]
17. Lee, H.E.; Park, J.H.; Jang, D.; Shin, J.H.; Im, T.H.; Lee, J.H.; Hong, S.K.; Wang, H.S.; Kwak, M.S.; Peddigari, M.; et al. Optogenetic brain neuromodulation by stray magnetic field via flash-enhanced magneto-mechano-triboelectric nanogenerator. *Nano Energy* **2020**, *75*, 104951. [CrossRef]
18. Jeong, Y.; Lee, H.E.; Shin, A.; Kim, D.; Lee, K.J.; Kim, D. Progress in Brain-Compatible Interfaces with Soft Nanomaterials. *Adv. Mater.* **2020**, *32*, 1907522. [CrossRef] [PubMed]
19. Park, J.H.; Seo, J.; Kim, C.; Joe, D.J.; Lee, H.E.; Im, T.H.; Seok, J.Y.; Jeong, C.K.; Ma, B.S.; Park, H.K.; et al. Flash-Induced Stretchable Cu Conductor via Multiscale-Interfacial Couplings. *Adv. Sci.* **2018**, *5*, 1801146. [CrossRef] [PubMed]
20. Hwang, I.; Kim, H.N.; Seong, M.; Lee, S.-H.; Kang, M.; Yi, H.; Bae, W.G.; Kwak, M.K.; Jeong, H.E. Multifunctional Smart Skin Adhesive Patches for Advanced Health Care. *Adv. Healthc. Mater.* **2018**, *7*, 1800275. [CrossRef]
21. Sreenilayam, S.P.; Ahad, I.U.; Nicolosi, V.; Acinas Garzon, V.; Brabazon, D. Advanced materials of printed wearables for physiological parameter monitoring. *Mater. Today* **2020**, *32*, 147–177. [CrossRef]
22. Jin, H.; Abu-Raya, Y.S.; Haick, H. Advanced Materials for Health Monitoring with Skin-Based Wearable Devices. *Adv. Healthc. Mater.* **2017**, *6*, 1700024. [CrossRef] [PubMed]
23. Lo, L.; Shi, H.; Wan, H.; Xu, Z.; Tan, X.; Wang, C. Inkjet-Printed Soft Resistive Pressure Sensor Patch for Wearable Electronics Applications. *Adv. Mater. Technol.* **2020**, *5*, 1900717. [CrossRef]
24. Yang, J.C.; Mun, J.; Kwon, S.Y.; Park, S.; Bao, Z.; Park, S. Electronic Skin: Recent Progress and Future Prospects for Skin-Attachable Devices for Health Monitoring, Robotics, and Prosthetics. *Adv. Mater.* **2019**, *31*, 1904765. [CrossRef] [PubMed]
25. Yeon, H.; Lee, H.; Kim, Y.; Lee, D.; Lee, Y.; Lee, J.S.; Shin, J.; Choi, C.; Kang, J.H.; Suh, J.M.; et al. Long-term reliable physical health monitoring by sweat pore–inspired perforated electronic skins. *Sci. Adv.* **2021**, *7*, 1–11. [CrossRef] [PubMed]
26. Xi, D.; Xiao, M.; Cao, J.; Zhao, L.; Xu, N.; Long, S.; Fan, J.; Shao, K.; Sun, W.; Yan, X.; et al. NIR Light-Driving Barrier-Free Group Rotation in Nanoparticles with an 88.3% Photothermal Conversion Efficiency for Photothermal Therapy. *Adv. Mater.* **2020**, *32*, 1907855. [CrossRef]
27. Xu, X.; Chen, J.; Cai, S.; Long, Z.; Zhang, Y.; Su, L.; He, S.; Tang, C.; Liu, P.; Peng, H.; et al. A Real-Time Wearable UV-Radiation Monitor based on a High-Performance p-CuZnS/n-$TiO_2$ Photodetector. *Adv. Mater.* **2018**, *30*, 1803165. [CrossRef]
28. Wang, C.; Xia, K.; Zhang, Y.; Kaplan, D.L. Silk-Based Advanced Materials for Soft Electronics. *Acc. Chem. Res.* **2019**, *52*, 2916–2927. [CrossRef]
29. Zodrow, K.R.; Li, Q.; Buono, R.M.; Chen, W.; Daigger, G.; Dueñas-Osorio, L.; Elimelech, M.; Huang, X.; Jiang, G.; Kim, J.-H.; et al. Advanced Materials, Technologies, and Complex Systems Analyses: Emerging Opportunities to Enhance Urban Water Security. *Environ. Sci. Technol.* **2017**, *51*, 10274–10281. [CrossRef]
30. Cai, S.; Xu, X.; Yang, W.; Chen, J.; Fang, X. Materials and Designs for Wearable Photodetectors. *Adv. Mater.* **2019**, *31*, 1808138. [CrossRef]
31. Lee, H.E.; Choi, J.H.; Lee, S.H.; Jeong, M.; Shin, J.H.; Joe, D.J.; Kim, D.H.; Kim, C.W.; Park, J.H.; Lee, J.H.; et al. Monolithic Flexible Vertical GaN Light-Emitting Diodes for a Transparent Wireless Brain Optical Stimulator. *Adv. Mater.* **2018**, *30*, 1–10. [CrossRef]
32. Jeong, C.K.; Park, K.-I.; Son, J.H.; Hwang, G.-T.; Lee, S.H.; Park, D.Y.; Lee, H.E.; Lee, H.K.; Byun, M.; Lee, K.J. Self-powered fully-flexible light-emitting system enabled by flexible energy harvester. *Energy Environ. Sci.* **2014**, *7*, 4035–4043. [CrossRef]

33. Lee, H.E.; Lee, S.H.; Jeong, M.; Shin, J.H.; Ahn, Y.; Kim, D.; Oh, S.H.; Yun, S.H.; Lee, K.J. Trichogenic Photostimulation Using Monolithic Flexible Vertical AlGaInP Light-Emitting Diodes. *ACS Nano* **2018**, *12*, 9587–9595. [CrossRef]
34. Lee, H.E.; Lee, D.; Lee, T.; Ho, J.; Choi, G. Wireless Powered Wearable Micro Light-Emitting Diodes. *Nano Energy* **2018**, in press. [CrossRef]
35. Shin, J.H.; Park, J.H.; Seo, J.; Im, T.H.; Kim, J.C.; Lee, H.E.; Kim, D.H.; Woo, K.Y.; Jeong, H.Y.; Cho, Y.; et al. A Flash-Induced Robust Cu Electrode on Glass Substrates and Its Application for Thin-Film μLEDs. *Adv. Mater.* **2021**, *33*, 2007186. [CrossRef] [PubMed]
36. Woodgate, G.J.; Harrold, J. P-101: Micro-Optical Systems for Micro-LED Displays. *SID Symp. Dig. Tech. Pap.* **2018**, *49*, 1559–1562. [CrossRef]
37. Marinov, V.R.; Swenson, O.; Atanasov, Y.; Schneck, N. Laser-assisted ultrathin die packaging: Insights from a process study. *Microelectron. Eng.* **2013**, *101*, 23–30. [CrossRef]
38. Kim, R.-H.; Bae, M.; Kim, D.G.; Cheng, H.; Kim, B.H.; Kim, D.-H.; Li, M.; Wu, J.; Du, F.; Kim, H.-S.; et al. Stretchable, Transparent Graphene Interconnects for Arrays of Microscale Inorganic Light Emitting Diodes on Rubber Substrates. *Nano Lett.* **2011**, *11*, 3881–3886. [CrossRef]
39. Kim, T.; Jung, Y.H.; Song, J.; Kim, D.; Li, Y.; Kim, H.; Song, I.-S.; Wierer, J.J.; Pao, H.A.; Huang, Y.; et al. High-Efficiency, Microscale GaN Light-Emitting Diodes and Their Thermal Properties on Unusual Substrates. *Small* **2012**, *8*, 1643–1649. [CrossRef]
40. Lee, S.H.; Kim, J.; Shin, J.H.; Lee, H.E.; Kang, I.-S.; Gwak, K.; Kim, D.-S.; Kim, D.; Lee, K.J. Optogenetic control of body movements via flexible vertical light-emitting diodes on brain surface. *Nano Energy* **2018**, *44*, 447–455. [CrossRef]
41. Mao, D.; Li, N.; Xiong, Z.; Sun, Y.; Xu, G. Single-Cell Optogenetic Control of Calcium Signaling with a High-Density Micro-LED Array. *iScience* **2019**, *21*, 403–412. [CrossRef] [PubMed]
42. Kim, W.S.; Hong, S.; Gamero, M.; Jeevakumar, V.; Smithhart, C.M.; Price, T.J.; Palmiter, R.D.; Campos, C.; Park, S. Il Organ-specific, multimodal, wireless optoelectronics for high-throughput phenotyping of peripheral neural pathways. *Nat. Commun.* **2021**, *12*, 157. [CrossRef]
43. Dieter, A.; Duque-Afonso, C.J.; Rankovic, V.; Jeschke, M.; Moser, T. Near physiological spectral selectivity of cochlear optogenetics. *Nat. Commun.* **2019**, *10*, 1962. [CrossRef]
44. Gutruf, P.; Yin, R.T.; Lee, K.B.; Ausra, J.; Brennan, J.A.; Qiao, Y.; Xie, Z.; Peralta, R.; Talarico, O.; Murillo, A.; et al. Wireless, battery-free, fully implantable multimodal and multisite pacemakers for applications in small animal models. *Nat. Commun.* **2019**, *10*, 5742. [CrossRef] [PubMed]
45. Cho, Y.; Park, J.; Lee, C.; Lee, S. Recent progress on peripheral neural interface technology towards bioelectronic medicine. *Bioelectron. Med.* **2020**, *6*, 23. [CrossRef]
46. Yu, K.; Niu, X.; He, B. Neuromodulation Management of Chronic Neuropathic Pain in the Central Nervous System. *Adv. Funct. Mater.* **2020**, *30*, 1908999. [CrossRef] [PubMed]
47. Naser Moghadasi, A. Neural implant for the treatment of multiple sclerosis. *Med. Hypotheses* **2020**, *145*, 110324. [CrossRef] [PubMed]
48. Hwang, G.-T.; Park, H.; Lee, J.-H.; Oh, S.; Park, K.-I.; Byun, M.; Park, H.; Ahn, G.; Jeong, C.K.; No, K.; et al. Self-Powered Cardiac Pacemaker Enabled by Flexible Single Crystalline PMN-PT Piezoelectric Energy Harvester. *Adv. Mater.* **2014**, *26*, 4880–4887. [CrossRef]
49. Hwang, G.-T.; Kim, Y.; Lee, J.-H.; Oh, S.; Jeong, C.K.; Park, D.Y.; Ryu, J.; Kwon, H.; Lee, S.-G.; Joung, B.; et al. Self-powered deep brain stimulation via a flexible PIMNT energy harvester. *Energy Environ. Sci.* **2015**, *8*, 2677–2684. [CrossRef]
50. Deisseroth, K. Optogenetics. *Nat. Methods* **2011**, *8*, 26–29. [CrossRef] [PubMed]
51. Boyden, E.S. Optogenetics and the future of neuroscience. *Nat. Neurosci.* **2015**, *18*, 1200–1201. [CrossRef]
52. Park, S.I.; Brenner, D.S.; Shin, G.; Morgan, C.D.; Copits, B.A.; Chung, H.U.; Pullen, M.Y.; Noh, K.N.; Davidson, S.; Oh, S.J.; et al. Soft, stretchable, fully implantable miniaturized optoelectronic systems for wireless optogenetics. *Nat. Biotechnol.* **2015**, *33*, 1280–1286. [CrossRef]
53. Shin, G.; Gomez, A.M.; Al-Hasani, R.; Jeong, Y.R.; Kim, J.; Xie, Z.; Banks, A.; Lee, S.M.; Han, S.Y.; Yoo, C.J.; et al. Flexible Near-Field Wireless Optoelectronics as Subdermal Implants for Broad Applications in Optogenetics. *Neuron* **2017**, *93*, 509–521.e3. [CrossRef]
54. Tajima, K.; Ikeda, K.; Tanabe, Y.; Thomson, E.A.; Yoneshiro, T.; Oguri, Y.; Ferro, M.D.; Poon, A.S.Y.; Kajimura, S. Wireless optogenetics protects against obesity via stimulation of non-canonical fat thermogenesis. *Nat. Commun.* **2020**, *11*, 1730. [CrossRef] [PubMed]
55. Kim, J.; Gutruf, P.; Chiarelli, A.M.; Heo, S.Y.; Cho, K.; Xie, Z.; Banks, A.; Han, S.; Jang, K.; Lee, J.W.; et al. Miniaturized Battery-Free Wireless Systems for Wearable Pulse Oximetry. *Adv. Funct. Mater.* **2017**, *27*, 1604373. [CrossRef] [PubMed]
56. Kim, J.; Salvatore, G.A.; Araki, H.; Chiarelli, A.M.; Xie, Z.; Banks, A.; Sheng, X.; Liu, Y.; Lee, J.W.; Jang, K.; et al. Battery-free, stretchable optoelectronic systems for wireless optical characterization of the skin. *Sci. Adv.* **2016**, *2*, e1600418. [CrossRef] [PubMed]